Extracting stochastic stress intensity factors using generalized polynomial chaos

Netta Omer[a], Zohar Yosibash[b]

[a]*Department of Mechanical Engineering, Afeka College of Engineering, Tel-Aviv, Israel*
[b]*School of Mechanical Engineering, The Iby and Aladar Fleischman Faculty of Engineering, Tel-Aviv University, Ramat-Aviv, Israel*

Abstract

Realistic material properties, as the Young modulus E and Poisson ratio ν (isotropic materials), are measured by experimental observations and are inherently stochastic. Having their stochastic representation $E(\xi)$ or $\nu(\xi)$ where ξ is a random variable, we formulate the elastic solution of the stochastic elasticity system in the vicinity of a crack tip.

We show that the stochastic asymptotic displacements are of the form

$$\boldsymbol{u}(r,\theta;\xi) = A_{01}(\xi)\boldsymbol{\varphi}^{(01)}(\theta;\xi)+A_{02}(\xi)\boldsymbol{\varphi}^{(02)}(\theta;\xi)+A_1(\xi)r^{1/2}\boldsymbol{\varphi}^{(1)}(\theta;\xi)+A_2(\xi)r^{1/2}\boldsymbol{\varphi}^{(2)}(\theta;\xi)+\mathcal{O}(r)$$

with deterministic eigenvalues and either deterministic or stochastic eigenfunctions $\boldsymbol{\varphi}^{(i)}(\theta;\xi)$ and coefficients A_i. However, the stresses are represented by an asymptotic series with a stochastic behavior manifested only in the SIF:

$$\boldsymbol{\sigma}(r,\theta;\xi) = \frac{K_I(\xi)}{\sqrt{2\pi r}}\boldsymbol{\phi}^{(1)}(\theta) + \frac{K_{II}(\xi)}{\sqrt{2\pi r}}\boldsymbol{\phi}^{(2)}(\theta) + \mathcal{O}(1)$$

We present explicitly whether the expressions in series expansions are stochastic or not, depending both on the material properties and on the boundary conditions far from the crack faces. The generalized polynomial chaos (GPC) method is used thereafter to compute the stochastic expressions from deterministic finite element solutions. As an example we consider either a stochastic Young modulus or Poisson ratio to be given as random variable with a normal distribution:

$$E(\xi) = E_0 + E_1\xi, \quad \text{or} \quad \nu(\xi) = \nu_0 + \nu_1\xi, \quad \xi \sim \mathcal{N}(0,\sigma^2)$$

Numerical examples are presented in which we compute $\varphi_i(\theta;\xi)$ and thereafter $A_i(\xi)$ and $K_I(\xi)$ from deterministic finite element analyses using the GPC. Monte Carlo simulations are used to demonstrate the efficiency of the proposed methods. Numerical examples are provided that show the efficiency and accuracy of the proposed methods.

Preprint submitted to Engineering Fracture Mechanics *November 28, 2018*

Keywords: Generalized polynomial chaos, Stochastic stress intensity factors

1. Introduction

Linear elastic fracture mechanics is a mature theory, based on stress intensity factors (SIFs denoted by K) in 2D domains, that allows to predict fracture initiation in the presence of cracks or crack propagation under cyclic loading. For isotropic materials, the SIFs depend on the boundary conditions and the geometry of the domain, and also on the material properties, the Young modulus E and Poisson ratio ν. Since experimental observations usually lead to a spread in E and ν measurements, their representation include randomness $E(\xi)$ and $\nu(\xi)$ where ξ is a random variable. As a result, this randomness is manifested in the SIFs. Herein we aim at investigating the representation of the stochastic solution in the vicinity of a crack tip, and especially the computation of the stochastic stress intensity factors (SSIF $K(\xi)$) in two-dimensional domains with a crack having stochastic material properties. We employ the generalized polynomial chaos (GPC) to address the stochastic nature of the problem, which is a very efficient method to solve stochastic partial differential equations [1, 2] at a fraction of the computational cost compared to Monte Carlo simulations.

Many publications focus on the SIF computation for cracked configuration due to uncertainties in crack geometry, load and material properties. In such cases the probability density function of crack growth is estimated based on a crack-instability criterion: Rahman, [3], addresses the computation of stochastic J-Rice integral using the finite element method (FEM), by using the stochastic representation of the crack geometry. Rao & Rahman, [4], compute the SSIF using a Galerkin meshless method for uncertainty in the crack geometry. Chowdhury, Song & Gao, [5], extract SSIFs using Monte-Carlo simulations by rescaling the crack size according to its stochastic presentation. Reddy & Rao, [6], use the continuum shape sensitivity analysis to evaluate the sensitivity of the fracture parameters in cases of mix-mode loading of cracks. Su & Zheng, [7], use the spline fictitious boundary element method to evaluate the SSIF in case of mode I and mixed-mode loading of cracks. These investigations focused on uncertainties in crack geometry and involves Monte-Carlo simulations, known to require exhaust computer resources due to their slow convergence rates.

Beck and Gomes, [8], used the polynomial chaos to obtain accurate representations of random crack propagation data. The analytical polynomial chaos representations derived were shown to well predict the reliability of structural components subject to fatigue.

The influence of randomness in material properties on the life of structures weakened by growing cracks has been of major interest in the engineering community, associated with the reliability estimates of structural components. Many publications focused on ceramics domains with uncertainties in material properties. Silberschmidt, [9], investigated the crack propagation in view of macroscopic failure manifestation. The method involves the computation of the SIF's however these are considered deterministic in the crack propagation simulation. Another macroscopic approach is presented by Keles, Garcia & Bowman [10] for brittle materials in which the $2D$ stress field and SIF's are computed using Monte-Carlo simulations.

Herein, we first analyze the asymptotic expansion of displacements and stresses in the vicinity of the crack tip and identify the quantities that are affected by the stochastic representation of $E(\xi)$ and $\nu(\xi)$. Thereafter, we employ the GPC [1, 2] to determine the various stochastic quantities that allows one to compute the SSIFs efficiently and accurately. Since the GPC results in a set of deterministic problems, each requiring to extraction of the SIFs for given deterministic material properties, we apply the quasi-dual function method (QDFM) for the extraction of the SIFs. Details on the QDFM (that is a general method for 3D domains with edge cracks) and its implementation may be found in [11],[12], [13]. The QDFM is accurate and efficient, implemented as a post-solution operation in conjunction with the p-version finite element method.

The paper is organized as follows: In Section 2 the statement of the problem of interest and necessary notations are provided. Explicitly, the asymptotic expansion of the displacements and stresses in the vicinity of a 2D crack tip in a linear elasticity isotropic and homogeneous domain is given by (see [14]):

$$\boldsymbol{u} = (u_r \ u_\theta)^T = A_{01}\boldsymbol{\varphi}^{(01)}(\theta) + A_{02}\boldsymbol{\varphi}^{(02)}(\theta) + A_1 r^{1/2}\boldsymbol{\varphi}^{(1)}(\theta) + A_2 r^{1/2}\boldsymbol{\varphi}^{(2)}(\theta) + \mathcal{O}(r) \qquad (1)$$

$$\boldsymbol{\sigma} = (\sigma_{rr} \ \sigma_{\theta\theta} \ \sigma_{r\theta})^T = \frac{K_I}{\sqrt{2\pi r}}\boldsymbol{\phi}^{(1)}(\theta) + \frac{K_{II}}{\sqrt{2\pi r}}\boldsymbol{\phi}^{(2)}(\theta) + \mathcal{O}(1) \qquad (2)$$

where K_i are the stress intensity factors (SIF) and the A_i are the displacements associated SIFs and $\boldsymbol{\varphi}^{(i)}(\theta), \boldsymbol{\phi}^{(i)}(\theta)$ are the well known eigenfunction. We identify in the displacements

and stresses asymptotic series (1) and (2) which are the quantities that are stochastic due to the stochastic representation of the material properties. The GPC for the computation of these quantities is formulated in Section 3, based on which we present the determination of the SSIFs. Section 4 provides four example problems to demonstrate the presented methods:

Example 1: A cracked circular domain with deterministic traction boundary conditions on the outer surface and E stochastic. We demonstrate that for this case A_i are stochastic but the eigenfunctions and K_i are deterministic. GPC convergence is compared to MC convergence in terms of number of Hermite polynomials used to span the stochastic space and in terms of p.

Example 2: A cracked circular domain with traction free crack faces, deterministic essential boundary conditions on the outer surface and E stochastic. We demonstrate that A_i are deterministic, however the stresses are stochastic as well as K_i.

Example 3: A cracked circular domain with traction free crack faces, deterministic essential boundary conditions on the outer surface of the domain and ν stochastic. We demonstrate that A_i are stochastic, eigenfunctions are stochastic as well as K_i.

Example 4: A realistic compact tension specimen (CTS) with deterministic traction boundary condition (bearing traction boundary conditions on the holes) and ν stochastic.

We conclude the paper by a summary and conclusions in Section 5.

2. Problem statement and notations

The departing point is the two dimensional linear elastic problem in an isotropic domain containing a crack. We seek for the displacements $\boldsymbol{u}(r,\theta) \overset{\text{def}}{=} (u_r \; u_\theta)^T$ that are the solution to the Navier-Lamè system of PDEs, assuming a **plane strain condition**, without body forces in a 2D domain $\Omega \subset \mathbb{R}^2$ containing a crack, see Figure 1:

$$2(\nu-1)\left(u_r - r\frac{\partial u_r}{\partial r} - r^2\frac{\partial^2 u_r}{\partial r^2}\right) + (1-2\nu)\frac{\partial^2 u_r}{\partial \theta^2} + (4\nu-3)\frac{\partial u_\theta}{\partial \theta} + r\frac{\partial^2 u_\theta}{\partial r \partial \theta} = 0 \tag{3}$$

$$r\frac{\partial^2 u_r}{\partial r \partial \theta} - (4\nu-3)\frac{\partial u_r}{\partial \theta} - 2(\nu-1)\frac{\partial^2 u_\theta}{\partial \theta^2} + (2\nu-1)\left(u_\theta - r\frac{\partial u_\theta}{\partial r} - r^2\frac{\partial^2 u_\theta}{\partial r^2}\right) = 0 \tag{4}$$

On crack faces, $\Gamma_1 \cup \Gamma_2$ that intersect at the crack tip $\mathcal{P}$, **traction free boundary conditions** are considered. The stresses $\boldsymbol{\sigma} \overset{\text{def}}{=} (\sigma_{rr} \; \sigma_{\theta\theta} \; \sigma_{r\theta})^T$ are obtained from the displacements

via the kinematic relationships and Hooke's law:

$$\boldsymbol{\sigma} = \frac{E}{(1+\nu)(1-2\nu)} \begin{Bmatrix} (1-\nu)\frac{\partial u_r}{\partial r} + \nu\frac{u_r}{r} + \nu\frac{1}{r}\frac{u_\theta}{\partial\theta} \\ \nu\frac{\partial u_r}{\partial r} + (1-\nu)\frac{u_r}{r} + (1-\nu)\frac{1}{r}\frac{u_\theta}{\partial\theta} \\ \frac{(1-2\nu)}{2}\left(\frac{1}{r}\frac{\partial u_r}{\partial\theta} - \frac{u_\theta}{r} + \frac{u_\theta}{\partial r}\right) \end{Bmatrix} \tag{5}$$

On the outer domain's boundary $\partial\Omega - \Gamma_1 - \Gamma_2$ either deterministic traction or deterministic displacements boundary conditions are prescribed:

$$\boldsymbol{\sigma}\cdot\boldsymbol{n} = \boldsymbol{t} \qquad \text{or} \qquad \boldsymbol{u} = \hat{\boldsymbol{u}} \qquad \text{on } \partial\Omega - \Gamma_1 - \Gamma_2 \tag{6}$$

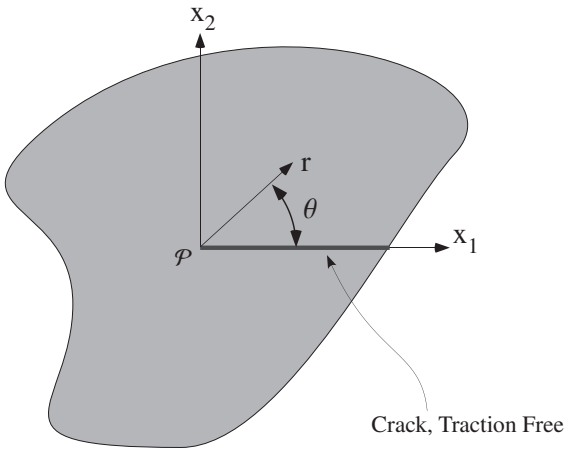

Figure 1: Cracked Domain of interest Ω.

Williams series in the vicinity of $\mathcal{P}$ in terms of eigenfunctions $(\boldsymbol{\varphi}_i(\theta))$ and their coefficients (A_i) are explicitly expressed as:

$$\begin{aligned} \boldsymbol{u} \;=\; & A_{01}\begin{Bmatrix} (4-4\nu)\sin(\theta) \\ (4-4\nu)\cos(\theta) \end{Bmatrix} + A_{02}\begin{Bmatrix} (4-4\nu)\cos(\theta) \\ (2-4\nu)\sin(\theta) \end{Bmatrix} \\ & + A_1 r^{1/2}\begin{Bmatrix} \sin\left(\frac{3\theta}{2}\right) + (5-8\nu)\sin\left(\frac{\theta}{2}\right) \\ \cos\left(\frac{3\theta}{2}\right) + (7-8\nu)\cos\left(\frac{\theta}{2}\right) \end{Bmatrix} + A_2 r^{1/2}\begin{Bmatrix} \cos\left(\frac{3\theta}{2}\right) + \frac{1}{3}(5-8\nu)\cos\left(\frac{\theta}{2}\right) \\ -\sin\left(\frac{3\theta}{2}\right) - \frac{1}{3}(7-8\nu)\sin\left(\frac{\theta}{2}\right) \end{Bmatrix} + \mathcal{O}(r) \end{aligned} \tag{7}$$

In view of (7) and using (5), the stresses may be expressed by the eigenstresses $(\boldsymbol{\phi}_i(\theta))$ and the associated SIFs (K_i) by the classical expressions:

$$\boldsymbol{\sigma} \;=\; \frac{K_I}{\sqrt{2\pi r}}\begin{Bmatrix} \frac{1}{4}\sin\left(\frac{3\theta}{2}\right) + \frac{5}{4}\sin\left(\frac{\theta}{2}\right) \\ -\frac{1}{4}\sin\left(\frac{3\theta}{2}\right) + \frac{3}{4}\sin\left(\frac{\theta}{2}\right) \\ \frac{1}{4}\cos\left(\frac{3\theta}{2}\right) - \frac{1}{4}\cos\left(\frac{\theta}{2}\right) \end{Bmatrix} + \frac{K_{II}}{\sqrt{2\pi r}}\begin{Bmatrix} \frac{3}{4}\cos\left(\frac{3\theta}{2}\right) + \frac{5}{4}\cos\left(\frac{\theta}{2}\right) \\ -\frac{3}{4}\cos\left(\frac{3\theta}{2}\right) + \frac{3}{4}\cos\left(\frac{\theta}{2}\right) \\ -\frac{3}{4}\sin\left(\frac{3\theta}{2}\right) + \frac{1}{4}\sin\left(\frac{\theta}{2}\right) \end{Bmatrix} + \mathcal{O}(1) \tag{8}$$

where:

$$K_I = \frac{2\sqrt{2\pi}}{(1+\nu)} EA_1 \quad , \qquad K_{II} = \frac{2\sqrt{2\pi}}{3(1+\nu)} EA_2 \tag{9}$$

Since the material properties determined by experimentation are in practice probabilistic, and to further simplify our presentation, we consider the situation in which either the Young modulus E **or** the Poisson ratio ν are a stochastic variable with a normal distribution given by:

$$E(\xi) = \mu_E + \xi\sigma_E, \quad \nu \quad \text{with} \quad \xi \sim \mathcal{N}(0,1), \quad f_\xi(t) = \frac{1}{\sqrt{2\pi}} e^{-\frac{t^2}{2}} \tag{10a}$$

or

$$E, \quad \nu(\xi) = \mu_\nu + \xi\sigma_\nu, \quad \text{with} \quad \xi \sim \mathcal{N}(0,1), \quad f_\xi(t) = \frac{1}{\sqrt{2\pi}} e^{-\frac{t^2}{2}} \tag{10b}$$

where μ_E is the mean value of E and σ_E is the standard deviation of E, μ_ν is the mean value of ν and σ_ν is the standard deviation of ν. $f_\xi(t)$ is the probability density function.

Although E cannot have negative value realizations and a normal distribution is not a best choice (log normal is a better description), we use it for simplicity of presentation and negative E realization will be discarded.

2.1. The stochastic Williams series

We state two theorems and provide a heuristic proof:

Theorem 1. *Let $E(\xi)$ be a random variable and let ν be deterministic. Then eigenvalues α_i are deterministic, $\alpha_{01} = \alpha_{02} = 0, \alpha_1 = \alpha_2 = \frac{1}{2}$, and:*

a) For deterministic traction boundary conditions on $\partial\Omega - \Gamma_1 - \Gamma_2$ then $A_i(\xi)$ are random variables, $\boldsymbol{\varphi}^{(i)}(\theta)$, K_i and $\boldsymbol{\phi}^{(i)}(\theta)$ are deterministic. This implies that $\boldsymbol{u}(r,\theta;\xi)$ is stochastic whereas $\boldsymbol{\sigma}(r,\theta)$ is deterministic.

$$\boldsymbol{u}(r,\theta;\xi) = \sum_{i=01,02,1,2} A_i(\xi) r^{\alpha_i} \boldsymbol{\varphi}^{(i)}(\theta) + \mathcal{O}(r), \qquad \boldsymbol{\sigma}(r,\theta) = \sum_{i=1,2} \frac{K_i}{\sqrt{2\pi r}} \boldsymbol{\phi}^{(i)}(\theta) + \mathcal{O}(1)$$

b) For deterministic displacements boundary conditions on $\partial\Omega - \Gamma_1 - \Gamma_2$ then A_i, $\boldsymbol{\varphi}^{(i)}(\theta)$, and $\boldsymbol{\phi}^{(i)}(\theta)$ are deterministic and $K_i(\xi)$ is a random variable. This implies that $\boldsymbol{u}(r,\theta)$ is deterministic whereas $\boldsymbol{\sigma}(r,\theta;\xi)$ is stochastic.

$$\boldsymbol{u}(r,\theta) = \sum_{i=01,02,1,2} A_i r^{\alpha_i} \boldsymbol{\varphi}^{(i)}(\theta) + \mathcal{O}(r), \qquad \boldsymbol{\sigma}(r,\theta;\xi) = \sum_{i=1,2} \frac{K_i(\xi)}{\sqrt{2\pi r}} \boldsymbol{\phi}^{(i)}(\theta) + \mathcal{O}(1)$$

Theorem 2. *Let $\nu(\xi)$ be a random variable and let E be deterministic. Then eigenvalues α_i are deterministic $\alpha_{01} = \alpha_{02} = 0, \alpha_1 = \alpha_2 = \frac{1}{2}$, and:*

a) For deterministic traction boundary conditions on $\partial\Omega - \Gamma_1 - \Gamma_2$ then $A_i(\xi)$ and $\boldsymbol{\varphi}^{(i)}(\theta;\xi)$ are random variables, and K_i and $\boldsymbol{\phi}^{(i)}(\theta)$ are deterministic. This implies that $\boldsymbol{u}(r,\theta;\xi)$ is stochastic whereas $\boldsymbol{\sigma}(r,\theta)$ is deterministic.

$$\boldsymbol{u}(r,\theta;\xi) = \sum_{i=01,02,1,2} A_i(\xi) r^{\alpha_i} \boldsymbol{\varphi}^{(i)}(\theta;\xi) + \mathcal{O}(r), \qquad \boldsymbol{\sigma}(r,\theta) = \sum_{i=1,2} \frac{K_i}{\sqrt{2\pi r}} \boldsymbol{\phi}^{(i)}(\theta) + \mathcal{O}(1)$$

b) For deterministic displacements boundary conditions on $\partial\Omega - \Gamma_1 - \Gamma_2$ then $A_i(\xi)$, and $\boldsymbol{\varphi}^{(i)}(\theta;\xi)$ are random variables, but $\boldsymbol{u}(r,\theta)$ is deterministic. $\boldsymbol{\phi}^{(i)}(\theta)$ are deterministic but $K_i(\xi)$ are stochastic. This implies that $\boldsymbol{\sigma}(r,\theta;\xi)$ is stochastic.

$$\boldsymbol{u}(r,\theta) = \sum_{i=01,02,1,2} A_i(\xi) r^{\alpha_i} \boldsymbol{\varphi}^{(i)}(\theta;\xi) + \mathcal{O}(r), \qquad \boldsymbol{\sigma}(r,\theta;\xi) = \sum_{i=1,2} \frac{K_i(\xi)}{\sqrt{2\pi r}} \boldsymbol{\phi}^{(i)}(\theta) + \mathcal{O}(1)$$

Corollary 1. *The eigenstresses $\boldsymbol{\phi}^{(1)}(\theta)$, $\boldsymbol{\phi}^{(2)}(\theta)$, (8) are deterministic for any stochastic E and ν, and the stochastic behavior is only manifested in the SIFs.*

A heuristic proof of Theorems

Substituting the displacements field (7) into Navier-Lamè differential equations, (3)-(4), accompanied by traction free boundary conditions on both crack surfaces, we obtain an equation for the determination of the eigenvalues α_i that is independent of material properties (see e.g. [15]) and therefore the eigenvalues are deterministic for any choice of material properties: $\alpha_{01} = \alpha_{02} = 0, \alpha_1 = \alpha_2 = \frac{1}{2}$.

The eigenfunctions $\boldsymbol{\varphi}^{(i)}$ are independent of E and depend on ν (see (7)). This implies that for a stochastic $E(\xi)$ the eigenfunctions $\boldsymbol{\varphi}^{(i)}$ are deterministic, and for a stochastic $\nu(\xi)$ the eigenfunctions are stochastic $\boldsymbol{\varphi}^{(i)}(\theta;\xi)$.

Consider Theorem 1a), for which $E(\xi)$ is stochastic with deterministic traction boundary conditions. Since such a problem can be formulated by an Airy stress function without body forces, including deterministic traction boundary conditions that are independent of $E(\xi)$, one obtains a deterministic boundary value problem for the computation of the stresses. Therefore, the stresses are deterministic in the entire domain, and thus allow a deterministic expansion for Theorem 1a).

Because Hooke's law involves $E(\xi)$, and since the stresses are deterministic, implies that the displacements (obtained inevitably from the stresses) must be stochastic. But since the eigenpairs are deterministic, to obtain stochastic displacements imply that $A_i(\xi)$ must be stochastic, which concludes the proof of Theorem 1a).

Consider Theorem 1b), for which $E(\xi)$ is stochastic with deterministic displacements boundary conditions. A deterministic displacements solution satisfies the boundary conditions, and thus can be considered as the solution to the boundary value problem. Thus, the displacements in the vicinity of the crack tip are also deterministic and since the eigenpairs are deterministic (depend on ν but not on $E(\xi)$), then A_i must be deterministic, which proves the displacements expansion for Theorem 1b).

Because Hooke's law involves $E(\xi)$, and since displacements are deterministic then stresses must be stochastic (obtained inevitably from the displacements). The eigenstresses do not depend on the material properties, but since the SIF depend on $E(\xi)$ and A_i and ν are deterministic, then following (9) the SIFs are stochastic, which concludes the proof of Theorem 1b).

Consider Theorem 2a), for which $\nu(\xi)$ is stochastic with deterministic traction boundary conditions. Since such a problem can be formulated by an Airy stress function without body forces, including deterministic traction boundary conditions that are independent of $\nu(\xi)$, one obtains the stress solution that is deterministic, which proves the stress expansion for Theorem 2a).

Because Hooke's law involves $\nu(\xi)$, and since the stresses are deterministic the displacements (obtained inevitably from the stresses) must be stochastic. The eigenfunctions depend on $\nu(\xi)$ so these are stochastic, and $A_i(\xi)$ must be stochastic, because it is computed by a deterministic K_i, a deterministic E but a stochastic ν according to (9). This concludes the proof of Theorem 2a).

Consider Theorem 2b), for which $\nu(\xi)$ is stochastic with deterministic displacements boundary conditions. Since the eigenfunctions depend on $\nu(\xi)$ these are stochastic. The displacements have to be deterministic to satisfy deterministic boundary conditions, then $A_i(\xi)$ must be stochastic in such a way that the multiplication with the stochastic eigenfunction

will result in a deterministic displacements.

Having deterministic displacements and using Hooke's law that includes the stochastic $\nu(\xi)$, then the stress tensor must be stochastic. Because the eigenstresses do not depend on the material properties and are deterministic then, the SIFs must be stochastic to obtain a stochastic stress tensor, which concludes the proof of Theorem 2b). □

Following (9) the relationship between mode I & mode II SIFs and the A_is for plane-strain are given by:

In case $E(\xi)$ then:

$$K_I(\xi) = \frac{2\sqrt{2\pi}}{(1+\nu)} E(\xi) A_1(\xi) \quad , \qquad K_{II}(\xi) = \frac{2\sqrt{2\pi}}{3(1+\nu)} E(\xi) A_2(\xi) \tag{11}$$

and in case $\nu(\xi)$ then:

$$K_I(\xi) = \frac{2\sqrt{2\pi}}{(1+\nu(\xi))} E A_1(\xi) \quad , \qquad K_{II}(\xi) = \frac{2\sqrt{2\pi}}{3(1+\nu(\xi))} E A_2(\xi) \tag{12}$$

3. The Generalized Polynomial Chaos

Once determining explicitly the asymptotic representation of the stochastic solution in the vicinity of a crack tip, we apply the GPC method to extract the SSIFs by efficient and accurate methods. We first describe the GPC methods for the computation of the stochastic eigenfunctions. We then use the QDFM to extract the coefficients $A_i(\xi_k)$ from finite element solutions, i.e. the coefficients for the cracked problem solved deterministically for several material properties. We use the QDFM [11, 12, 13], although any method for the extraction of the A_i is appropriate. Having the stochastic representation of the eigenfunctions and $A_i(\xi_k)$, we present the methods to determine the stochastic SIFs (SSIFs). We conclude this section by methods to determine the different statistical moments of the SSIFs.

3.1. Approximating Eigenfunctions by GPC

A fast realization of $\boldsymbol{\varphi}(\theta;\xi)$ is achieved by the use of GPC. $\boldsymbol{\varphi}(\theta;\xi)$ is approximated in the stochastic space by projecting it into a stochastic finite dimensional space spanned by the Wiener-Hopf expansion. If $E(\xi)$ or $\nu(\xi)$ are represented by a normal distribution, then $\boldsymbol{\varphi}(\theta;\xi)$ is approximated by stochastic Hermite polynomials $He_n(\xi)$:

$$\boldsymbol{\varphi}^D(\theta;\xi) = \sum_{n=0}^{N-1} \boldsymbol{\varphi}_n^D(\theta)\, He_n(\xi) \tag{13}$$

where $\boldsymbol{\varphi}_n^D(\theta)$ are displacements computed with a deterministic value of E or ν (a specific ξ). The error between the exact and approximated eigenfunction is:

$$\begin{aligned} \boldsymbol{e}^{(\boldsymbol{\varphi})}(\theta;\xi) &= \boldsymbol{\varphi}(\theta;\xi) - \boldsymbol{\varphi}^D(\theta;\xi) \\ &= \boldsymbol{\varphi}(\theta;\xi) - \sum_{n=0}^{N-1} \boldsymbol{\varphi}_n^D(\theta) He_n(\xi) \end{aligned} \tag{14}$$

and since the error must be orthogonal to the Hermite polynomials space in the "mean norm" then $\mathbb{E}(\boldsymbol{e}^{(\boldsymbol{\varphi})}(X,\xi)He_k(\xi))$ must be zero:

$$\begin{aligned} \mathbb{E}(\boldsymbol{e}^{(\boldsymbol{\varphi})}(\theta;\xi)He_k(\xi)) &\equiv 0 \\ \mathbb{E}(\boldsymbol{e}^{(\boldsymbol{\varphi})}(\theta;\xi)He_k(\xi)) &= \int_{-\infty}^{\infty} \boldsymbol{e}^{(\boldsymbol{\varphi})}(\theta;t)He_k(t)f(t)dt \\ &= \int_{-\infty}^{\infty} \boldsymbol{e}^{(\boldsymbol{\varphi})}(\theta;t)He_k(t)\frac{1}{\sqrt{2\pi}}\boldsymbol{e}^{-\frac{t^2}{2}}dt \quad \forall k=0,\cdots,N-1 \\ &= \int_{-\infty}^{\infty} \left(\boldsymbol{\varphi}(\theta;t) - \sum_{n=0}^{N-1} \boldsymbol{\varphi}_n^D(\theta)He_n(t)\right) He_k(t)\frac{1}{\sqrt{2\pi}}e^{-\frac{t^2}{2}}dt \quad \forall k=0,\cdots,N-1 \end{aligned} \tag{15}$$

The RHS in (15) is zero, so one obtains:

$$\begin{aligned} \int_{-\infty}^{\infty} \boldsymbol{\varphi}(\theta;t)He_k(t)\frac{1}{\sqrt{2\pi}}e^{-\frac{t^2}{2}}dt &= \int_{-\infty}^{\infty} \sum_{n=0}^{N-1} \boldsymbol{\varphi}_n^D(\theta)He_n(t)He_k(t)\frac{1}{\sqrt{2\pi}}e^{-\frac{t^2}{2}}dt \quad \forall k=0,\cdots,N-1 \\ &= \sum_{n=0}^{N-1} \boldsymbol{\varphi}_n^D(\theta)\int_{-\infty}^{\infty} He_n(t)He_k(t)\frac{1}{\sqrt{2\pi}}e^{-\frac{t^2}{2}}dt \quad \forall k=0,\cdots,N-1 \\ &= \sum_{n=0}^{N-1} \boldsymbol{\varphi}_n^D(\theta)k!\delta_{nk} \quad \forall k=0,\cdots,N-1 \\ &= k!\boldsymbol{\varphi}_k^D(\theta) \quad \forall k=0,\cdots,N-1 \end{aligned}$$

Changing index k to n in (16) to comply with (13), each $\boldsymbol{\varphi}_n^D(\theta)$ may be computed by a deterministic expression:

$$\boldsymbol{\varphi}_n^D(\theta) = \frac{1}{n!}\int_{-\infty}^{\infty} \boldsymbol{\varphi}(\theta;t)He_n(t)\frac{1}{\sqrt{2\pi}}e^{-\frac{t^2}{2}}dt \tag{16}$$

The integral in (16) is computed by a Gauss-Hermite quadrature:

$$\begin{aligned} \boldsymbol{\varphi}_n^D(\theta) &\simeq \frac{1}{n!}\sum_{k=1}^{K} w_k e^{\xi_k^2}\boldsymbol{\varphi}(\theta;\xi_k)He_n(\xi_k)\frac{1}{\sqrt{2\pi}}e^{-\frac{\xi_k^2}{2}} \\ &= \frac{1}{\sqrt{2\pi}n!}\sum_{k=1}^{K} w_k e^{\frac{\xi_k^2}{2}}\boldsymbol{\varphi}(\theta;\xi_k)He_n(\xi_k) \end{aligned} \tag{17}$$

The eigenfunction $\boldsymbol{\varphi}(\theta;\xi_k)$ is a deterministic eigenfunction that must by computed for a given $E(\xi_k)$, and is obtained by a FE approximation denoted by $\boldsymbol{\varphi}^{FE}(\theta;\xi_k)$. In this case one finally obtains:

$$\boldsymbol{\varphi}^{D}(\theta;\xi) = \sum_{n=0}^{N-1}\left(\frac{1}{\sqrt{2\pi}n!}\sum_{k=1}^{K} w_k e^{\frac{\xi_k^2}{2}}\boldsymbol{\varphi}^{FE}(\theta;\xi_k)He_n(\xi_k)\right)He_n(\xi) \tag{18}$$

Here ξ_k are Gauss-Hermite abscissas (the roots of *physical* Hermite polynomials) and w_k are the corresponding weights. The abscissas ξ_k correspond to a deterministic Young modulus $E(\xi_k)$ or a deterministic Poisson ratio $\nu(\xi_k)$.

3.1.1. Representing $\boldsymbol{u}^D(r,\theta;\xi)$

The GPC can also be applied to the solution $\boldsymbol{u}(r,\theta;\xi)$, approximated it by stochastic Hermite polynomials $He_n(\xi)$:

$$\boldsymbol{u}^{D}(r,\theta;\xi) = \sum_{n=0}^{N-1}\boldsymbol{u}_n^{D}(r,\theta)\,He_n(\xi) \tag{19}$$

Following same steps as in subsection 3.1, one obtains:

$$\boldsymbol{u}_n^{D}(r,\theta) \simeq \frac{1}{\sqrt{2\pi}n!}\sum_{k=1}^{K} w_k e^{\frac{\xi_k^2}{2}}\boldsymbol{u}(r,\theta;\xi_k)He_n(\xi_k) \tag{20}$$

and again $\boldsymbol{u}(r,\theta;\xi_k)$ is replaced by a FE approximation $\boldsymbol{u}^{FE}(r,\theta;\xi_k)$ so the displacements are:

$$\boldsymbol{u}^{D}(r,\theta;\xi) = \sum_{n=0}^{N-1}\left(\frac{1}{\sqrt{2\pi}n!}\sum_{k=1}^{K} w_k e^{\frac{\xi_k^2}{2}}\boldsymbol{u}^{FE}(r,\theta;\xi_k)He_n(\xi_k)\right)He_n(\xi) \tag{21}$$

We note again that ξ_k are Gauss-Hermite abscissas corresponding to a deterministic $E(\xi_k)$ or $\nu(\xi_k)$.

On the other hand, having already a FE model of the domain with the crack of interest, we may use it not for the computation of $\boldsymbol{u}^{FE}(r,\theta;\xi_k)$, but instead to extract by the QDFM the coefficients $A_i(\xi_k)$ for the K material properties, be it $E(\xi_k)$ or $\nu(\xi_k)$. Having the coefficinets $A_i(\xi_k)$ computed and the eigenfunctions computed, $\boldsymbol{u}^{FE}(r,\theta;\xi_k)$ is represented by these expressions, and not computed by the FEA:

$$\boldsymbol{u}^{D}(r,\theta;\xi) = \sum_{n=0}^{N-1}\left(\frac{1}{\sqrt{2\pi}n!}\sum_{k=1}^{K} w_k e^{\frac{\xi_k^2}{2}}\left(\sum_{i\geq 1} A_i^{FE}(\xi_k)r^{\frac{1}{2}}\boldsymbol{\varphi}^{(i)}(\theta;\xi_k)\right)He_n(\xi_k)\right)He_n(\xi) \tag{22}$$

3.2. Computing $A_i(\xi)$, and consequently the SSIFs $K_I(\xi)$

The expression in (22) may be split into two separate displacements - these corresponding to mode I for $i = 1$:

$$\boldsymbol{u}^{(1)D}(r,\theta;\xi) = \sum_{n=0}^{N-1}\left(\frac{1}{\sqrt{2\pi}n!}\sum_{k=1}^{K} w_k e^{\frac{\xi_k^2}{2}}\left(A_1^{FE}(\xi_k) r^{\frac{1}{2}}\boldsymbol{\varphi}^{(1)}(\theta;\xi_k)\right) He_n(\xi_k)\right) He_n(\xi) \tag{23}$$

or these that correspond to the displacements related with mode II:

$$\boldsymbol{u}^{(2)D}(r,\theta;\xi) = \sum_{n=0}^{N-1}\left(\frac{1}{\sqrt{2\pi}n!}\sum_{k=1}^{K} w_k e^{\frac{\xi_k^2}{2}}\left(A_2^{FE}(\xi_k) r^{\frac{1}{2}}\boldsymbol{\varphi}^{(2)}(\theta;\xi_k)\right) He_n(\xi_k)\right) He_n(\xi) \tag{24}$$

On the other hand, according to Theorems 1-2, the displacements associated with mode I $\boldsymbol{u}^{(1)D}(r,\theta;\xi)$, and these associated with mode II $\boldsymbol{u}^{(2)D}(r,\theta;\xi)$ are also expressed as:

$$\boldsymbol{u}^{(1)D}(r,\theta,\xi) = A_1(\xi) r^{\frac{1}{2}}\boldsymbol{\varphi}^{(1)D}(\theta,\xi) \tag{25}$$

$$\boldsymbol{u}^{(2)D}(r,\theta,\xi) = A_2(\xi) r^{\frac{1}{2}}\boldsymbol{\varphi}^{(2)D}(\theta,\xi) \tag{26}$$

for any r,θ. Comparing (25) to (23), and (26) to (24), we may determine $A_1(\xi)$:

$$A_1(\xi) = \frac{u_r^{(1)D}(r,\theta,\xi)}{r^{\frac{1}{2}}\varphi_r^{(1)D}(\theta,\xi)} \quad \text{or} \qquad A_1(\xi) = \frac{u_\theta^{(1)D}(r,\theta,\xi)}{r^{\frac{1}{2}}\varphi_\theta^{(1)D}(\theta,\xi)} \tag{27}$$

as well as $A_2(\xi)$:

$$A_2(\xi) = \frac{u_r^{(2)D}(r,\theta,\xi)}{r^{\frac{1}{2}}\varphi_r^{(2)D}(\theta,\xi)} \quad \text{or} \qquad A_2(\xi) = \frac{u_\theta^{(2)D}(r,\theta,\xi)}{r^{\frac{1}{2}}\varphi_\theta^{(2)D}(\theta,\xi)} \tag{28}$$

Having $A_1(\xi)$ and $A_2(\xi)$ the SSIFs $K_I(\xi)$ and $K_{II}(\xi)$ are easily computed by (11)-(12).

In (27) and (28) an arbitrary r and arbitrary angle θ can be used, $(r,\theta) = (r_s,\theta_s)$ for which we may compute these expressions (either using displacement in r direction or θ direction). Both options and each arbitrary selected point should provide the exact same $A_1(\xi)$ and $A_2(\xi)$.

Finally, substituting (27), (28) in (11)-(12) at any given (r_s,θ_s), one obtains an explicit expression for the SSIFs in case of a stochastic $E(\xi)$:

$$\begin{aligned}
K_I(\xi) &= \frac{2\sqrt{2\pi}E(\xi)u_r^{(1)D}(r_s,\theta_s,\xi)}{(1+\nu)r_s^{\frac{1}{2}}\varphi_r^{(1)D}(\theta_s,\xi)} \quad \text{or} \qquad K_I(\xi) = \frac{2\sqrt{2\pi}E(\xi)u_\theta^{(1)D}(r_s,\theta_s,\xi)}{(1+\nu)r_s^{\frac{1}{2}}\varphi_\theta^{(1)D}(\theta_s,\xi)} \\
K_{II}(\xi) &= \frac{2\sqrt{2\pi}E(\xi)u_r^{(2)D}(r_s,\theta_s,\xi)}{3(1+\nu)r_s^{\frac{1}{2}}\varphi_r^{(2)D}(\theta_s,\xi)} \quad \text{or} \qquad K_{II}(\xi) = \frac{2\sqrt{2\pi}E(\xi)u_\theta^{(2)D}(r_s,\theta_s,\xi)}{3(1+\nu)r_s^{\frac{1}{2}}\varphi_\theta^{(2)D}(\theta_s,\xi)}
\end{aligned} \tag{29}$$

or in case of a stochastic $\nu(\xi)$:

$$K_I(\xi) = \frac{2\sqrt{2\pi}Eu_r^{(1)D}(r_s,\theta_s,\xi)}{(1+\nu(\xi))r_s^{\frac{1}{2}}\varphi_r^{(1)D}(\theta_s,\xi)} \quad \text{or} \qquad K_I(\xi) = \frac{2\sqrt{2\pi}Eu_\theta^{(1)D}(r_s,\theta_s,\xi)}{(1+\nu(\xi))r_s^{\frac{1}{2}}\varphi_\theta^{(1)D}(\theta_s,\xi)}$$
$$K_{II}(\xi) = \frac{2\sqrt{2\pi}Eu_r^{(2)D}(r_s,\theta_S,\xi)}{3(1+\nu(\xi))r_s^{\frac{1}{2}}\varphi_r^{(2)D}(\theta_s,\xi)} \quad \text{or} \qquad K_{II}(\xi) = \frac{2\sqrt{2\pi}Eu_\theta^{(2)D}(r_s,\theta_S,\xi)}{3(1+\nu(\xi))r_s^{\frac{1}{2}}\varphi_\theta^{(2)D}(\theta_s,\xi)} \tag{30}$$

Any statistical moment of the SSIFs (the mean, variance, skewness, kurtosis, etc) may be easily computed by the application of the Monte-Carlo method - randomly selected samples of ξ according to it's stochastic distribution is inserted in the RHS of (29)-(30).

4. Numerical Examples

We present herein four example problems used to compute stochastic eigenfunctions and SSIFs using the GPC with an increasing number of Hermite Polynomials N, and increasing number of Gauss-Hermite integration points, K to investigate the convergence of the solution in the stochastic space. We compare the solution obtained with the solution with the highest number of Hermite Polynomials: $N = 12$ and the highest number of Hermite Gauss points: $K = 25$. The mean value is independent of the number of Hermite Polynomials, N whereas the variance is dependent on both N and K. The relative difference in percentage of the computed eigenfunctions, mean and variance, are defined by:

$$\%\text{Difference}(\mu[\varphi_{(K)}^D]) = 100\left|\frac{\mu[\varphi_{(25)}^D] - \mu[\varphi_{(K)}^D]}{\mu[\varphi_{(25)}^D]}\right|$$
$$\%\text{Difference}(\sigma^2[\varphi_{(K,N)}^D]) = 100\left|\frac{\sigma^2[\varphi_{(25,12)}^D] - \sigma^2[\varphi_{(K,N)}^D]}{\sigma^2[\varphi_{(25,12)}^D]}\right| \tag{31}$$

The relative difference in percentage of the computed displacements, mean and variance, are defined by:

$$\%\text{Difference}(\mu[u_{(K)}^D]) = 100\left|\frac{\mu[u_{(25)}^D] - \mu[u_{(K)}^D]}{\mu[u_{(25)}^D]}\right|$$
$$\%\text{Difference}(\sigma^2[u_{(K,N)}^D]) = 100\left|\frac{\sigma^2[u_{(25,12)}^D] - \sigma^2[u_{(K,N)}^D]}{\sigma^2[u_{(25,12)}^D]}\right| \tag{32}$$

Once the SSIF are computed by the GPC method (using $\boldsymbol{u}^D(r,\theta;\xi)$ and $\boldsymbol{\varphi}^D(\theta;\xi)$), and by Monte-Carlo method, we compare the results of K_I computed using Monte-Carlo methos

with increasing number of samples to the result obtained using the GPC method using 12 Hermite Polynomials and 25 Gauss-Hermite integration points. The relative difference in percentage of the SSIF, mean and variance, are defined by:

$$\%\text{Difference}(\mu[K_I^{(MC)}]) = 100\left|\frac{\mu[K_I^{(GPC)}] - \mu[K_I^{(MC)}]}{\mu[K_I^{(GPC)}]}\right|$$
$$\%\text{Difference}(\sigma^2[K_I^{(MC)}]) = 100\left|\frac{\sigma^2[K_I^{(GPC)}] - \sigma^2[K_I^{(MC)}]}{\sigma^2[K_I^{(GPC)}]}\right| \tag{33}$$

We refer to the third and fourth moments as the centered, non-scaled moments. The scaled and centered third & fourth moments are the skewness & kurtosis respectively.

4.1. Cracked domain with stochastic Young modulus & deterministic traction BCs

Consider a cracked circular domain with radius 1 and with deterministic traction boundary conditions: $T_y = cos(\frac{\theta}{2})$ on the outer circular surface. Crack faces are traction free, as presented in Figure 2. The applied tractions are such that they excite only the term in the solution expansion associated with Mode I. We consider a stochastic Young modulus and

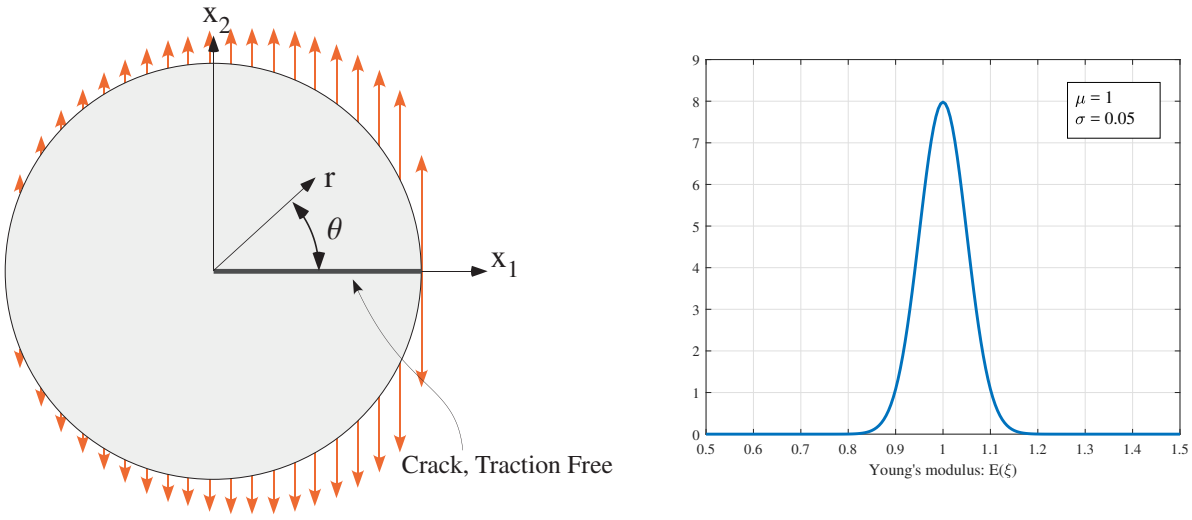

Figure 2: Left: The considered cracked domain having traction boundary conditions: $T_y = cos(\frac{\theta}{2})$. Right: Stochastic Young Modulus: $E = 1 + 0.05\xi$.

deterministic Poisson ratio:

$$E(\xi) = 1 + 0.05\xi, \quad \nu = 0.3$$
$$\xi \sim \mathcal{N}(0,1), \quad f_\xi(t) = \frac{1}{\sqrt{2\pi}} e^{-\frac{t^2}{2}} \tag{34}$$

so that **this example problem demonstrates a case according to Theorem 1(a)**.

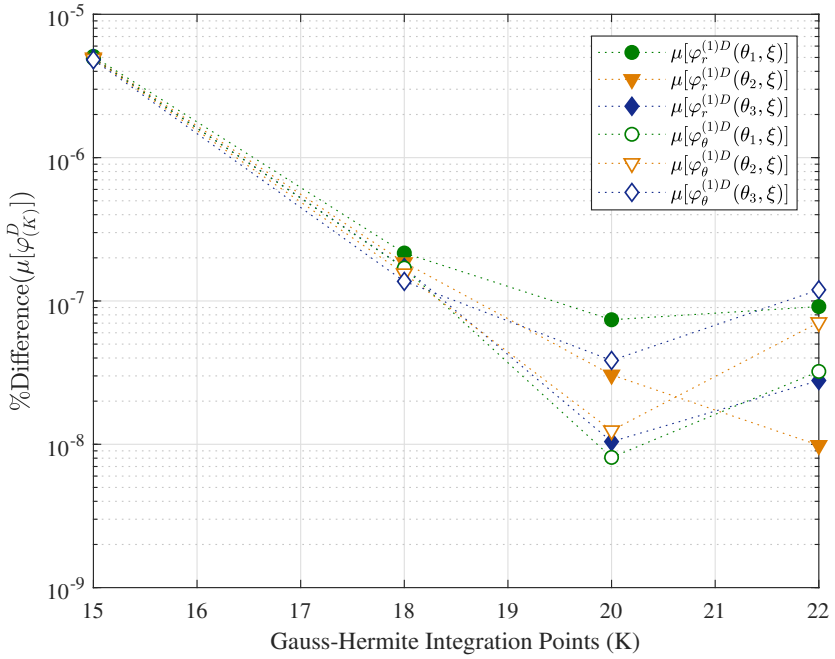

Figure 3: Relative difference of the mean value of $\boldsymbol{\varphi}^{(1)D}(\theta,\xi)$, (31), for increasing number of Gauss-Hermite integration points (K) at 3 arbitrary selected points. $\theta_1 = \frac{2}{9}\pi, \theta_2 = \frac{4}{9}\pi, \theta_3 = \frac{2}{3}\pi$.

4.1.1. Convergence of the eigenfunction: $\boldsymbol{\varphi}^{(1)D}(\theta;\xi)$

Following the steps presented in 3.1, we compute the eigenfunctions $\boldsymbol{\varphi}^{(1)D}(\theta;\xi)$. Since only E is stochastic, we expect the eigenfunctions $\boldsymbol{\varphi}^{(1)D}(\theta;\xi)$ to be deterministic. I.e., if we compute these as stochastic functions using increasing number of Gauss-Hermite integration points and increasing number of Hermite polynomials, we expect them to have a zero variance $\sigma^2 = 0$. The convergence of the mean value of $\boldsymbol{\varphi}^{(1)D}(\theta;\xi)$ is presented in figure 3 and the variance of $\boldsymbol{\varphi}_r^{(1)D}(\theta,\xi)$ & $\boldsymbol{\varphi}_\theta^{(1)D}(\theta;\xi)$, is below 10^{-15} as expected, the third moment obtained is less then 10^{-17} and the fourth moment obtained is less then 10^{-21}.

4.1.2. Convergence of the solution: $\boldsymbol{u}^{(1)D}(r,\theta;\xi)$

Since $\boldsymbol{u}^{(1)D}(r,\theta;\xi)$ is stochastic, we represent it by (23) using an increasing number of Hermite polynomials and an increasing number of Gauss-Hermite integration points. Once (23) is computed, it is used for computing the mean and variance of $\boldsymbol{u}^{(1)D}(r_s,\theta_s,\xi)$ (at three arbitrary locations). The convergence of the mean of $\boldsymbol{u}^{(1)D}$ is presented in Figure 4 and the convergence of the variance of $\boldsymbol{u}^{(1)D}$ is presented in Figures 5.

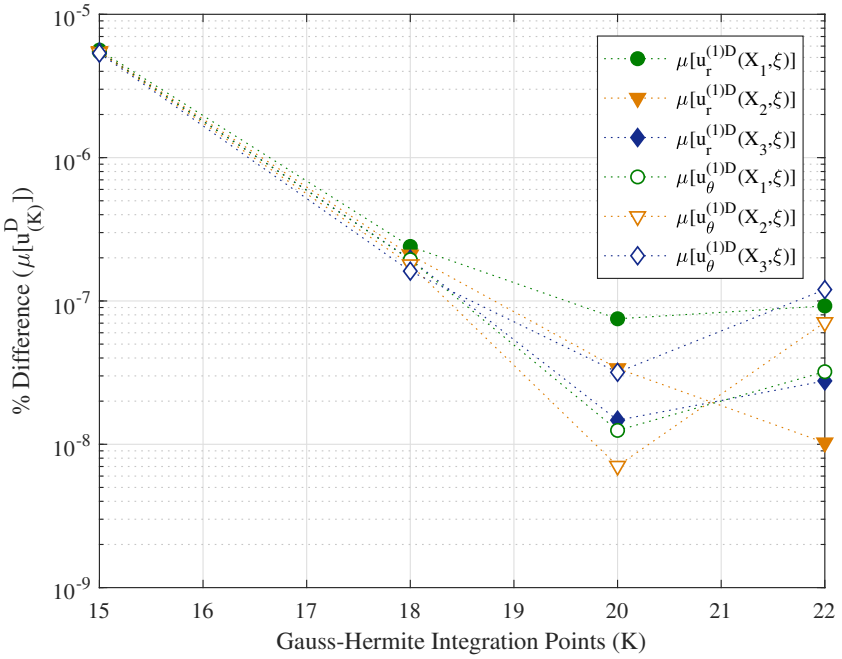

Figure 4: *Relative difference of the mean of the solution,* (32)*, for increasing number of Gauss-Hermite integration points (K) at* 3 *arbitrary selected points* $X_1 = (0.1, \frac{2}{9}\pi), X_2 = (0.1, \frac{4}{9}\pi), X_3 = (0.1, \frac{2}{3}\pi)$.

4.1.3. Computing the GSIF A_1

We selected 15 arbitrarily $(r_s, \theta_s$ points, and for each we computed $A_1(\xi)$ using both the displacements and eigenfunction in the r direction of and the θ direction (equation (27)). For each computation we used $500,000$ samples. All computations provide the same results:

$$\begin{aligned} \mu[A_1(\xi)] &= 2.29534286 \\ \sigma^2[A_1(\xi)] &= 0.01336857 \end{aligned} \tag{35}$$

The third and fourth moments of $A_1(\xi)$ are both lower then 10^{-4}. The probability density function (pdf) of A_1 is presented in Figure 6.

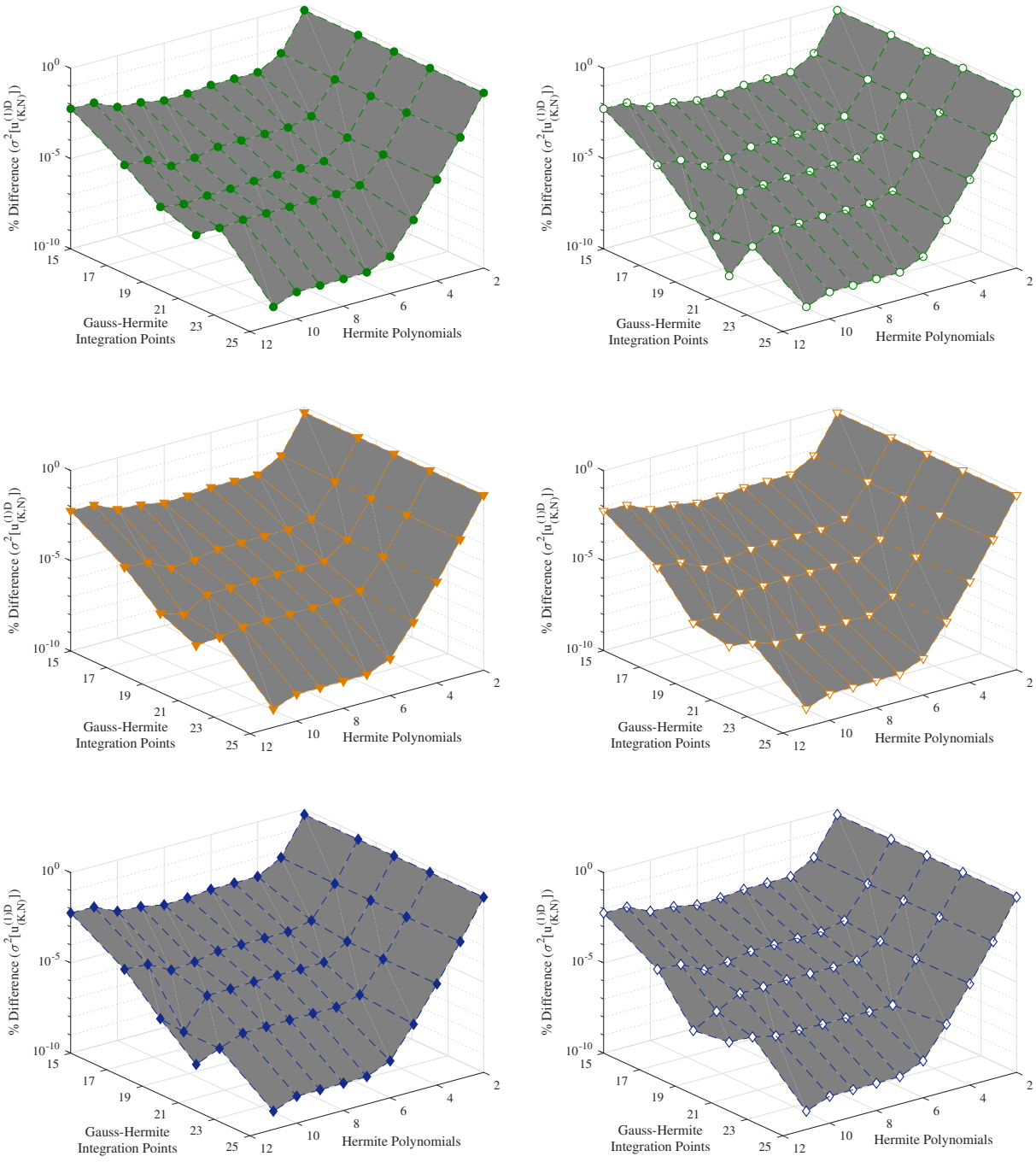

Figure 5: *Relative difference,* (32)*, of the variance of the solution as a function of the number of Hermite polynomials* (N) *and the number of Gauss-Hermite integration points* (K) *at* 3 *arbitrary selected points. Left:* $\boldsymbol{u}_r$*, Right:* $\boldsymbol{u}_\theta$*. Top:* $X = (0.1, \frac{2}{9}\pi), Center : X = (0.1, \frac{4}{9}\pi), Bottom : X = (0.1, \frac{2}{3}\pi)$.

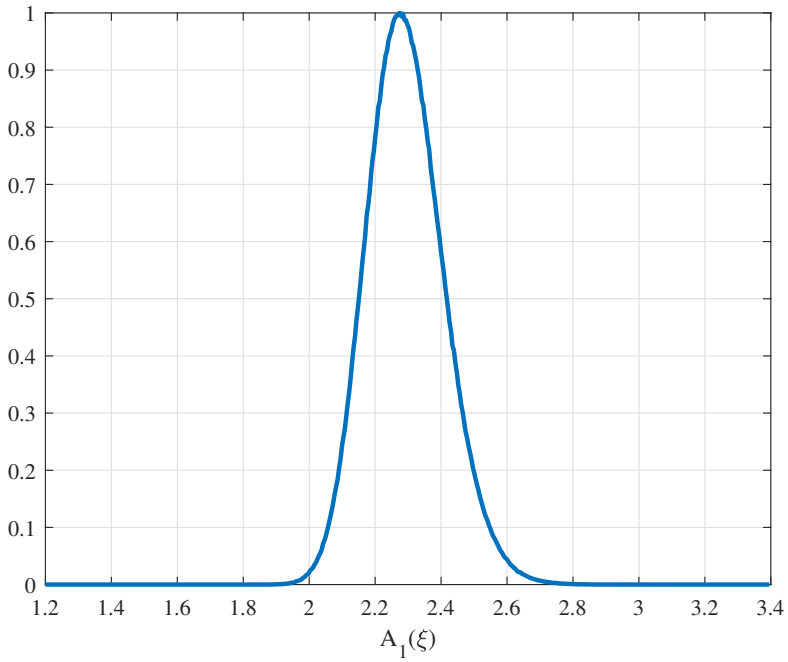

Figure 6: PDF of $A_1(\xi)$, computed using $u_r^{(1)D}(0.1, \frac{2}{9}\pi; \xi), \varphi_r^{(1)D}(\frac{2}{9}\pi; \xi)$.

4.1.4. Computing the SSIF K_I.

Having $A_1(\xi)$, we may compute the SSIF $K_I(\xi)$ using equation (11). We use 500000 samples and obtained the mean and variance:

$$\begin{aligned} \mu[K_I(\xi)] &= 8.82957684 \\ \sigma^2[K_I(\xi)] &= 7.05325764 \cdot 10^{-13} \end{aligned} \tag{36}$$

The third moment obtained is smaller than 10^{-17} (with skewness 0.30520373) and fourth moment of $K_I(\xi)$ is smaller than 10^{-21} (with kurtosis 3.19093056). The results indicate that although material properties are stochastic, herein the SSIF K_I is deterministic, as expected.

4.1.5. Comparison between the computed $K_I(\xi)$ and Monte-Carlo realization of $K_I(\xi)$.

Using the J-integral, [16], (at $R = 0.1$) finite element method and Monte-Carlo method, we extract the SSIF $K_I(\xi)$ for 10000 different choices of Young modulus, according to the stochastic behavior of $E(\xi)$, (34). All choices of Young modulus provide the same SSIF, as expected according to Theorem 1a. The relative difference of the mean value of the SSIF computed using Monte-Carlo method compared with the GPC method (equation (33)) is presented in Figure 7. Since the SSIF obtained is deterministic, it is not affected by the number of Monte Carlo realizations. Result show that the relative error obtained is less than 0.5%.

The variance of the SIF computed using Monte-Carlo method is less then 10^{-24}, the third moment is less then 10^{-34} (with skewness -1) and the fourth moment is less then 10^{-46} (with kurtosis 1), all are numerical zero, identical to the results obtained by the GPC method.

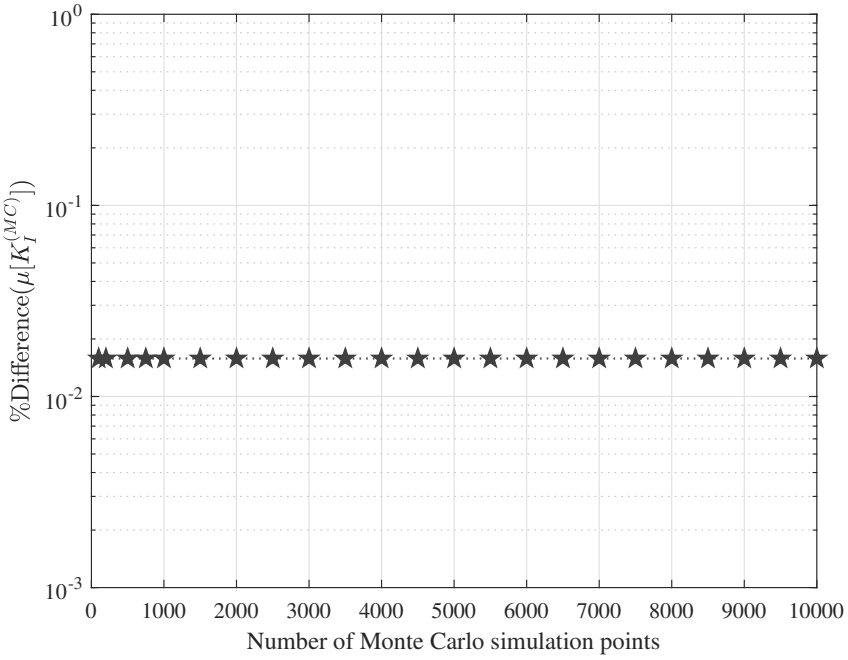

Figure 7: Relative difference of the mean value of the SSIF computed using increasing number of Monte-Carlo points vs. the SSIF computed using the GPC method, (33).

4.2. A Cracked domain with a stochastic Young modulus & displacements boundary conditions

Consider the same circular cracked domain as in Section 4.1, traction free boundary conditions on crack faces, same stochastic Young modulus and deterministic Poisson ratio as in (34), however, displacements boundary conditions are prescribed on the circular boundary $u_\theta(r=1) = \cos(\frac{\theta}{2})$, such that only Mode I is excited.

Following same steps as in Section 4.1, we compute the SIF using the GPC representation of the eigenfunctions. We perform the computation using several arbitrary selected points in the domain, all providing the same SSIF:

$$K_I(\xi) = 0.07793358 + 0.27916166\xi \tag{37}$$

where the third moment is less then 10^{-11} (with skewness 0.00074423) and the fourth moment is less then 10^{-10} (with kurtosis 3.00035850).

Using the J-integral (at $R = 0.1$), the finite element method and the Monte-Carlo method, we extract the SSIF $K_I(\xi)$ for 10000 different choices of Young modulus, according to the stochastic behavior of $E(\xi)$, (34). The results of $K_I(\xi)$ obtained at the 10000 samples are converged in both the mean value (less then 0.01%) and the variance (less then 0.4%). The PDF of the obtained SIF using both the GPC method and the Monte-Carlo method is presented in Figure 8.

The relative difference of the mean value and the variance of the SIF computed by Monte-Carlo method compared with the GPC method (equation (33)) is presented in Figure 9. Results show that the relative difference obtained is less then 2%.

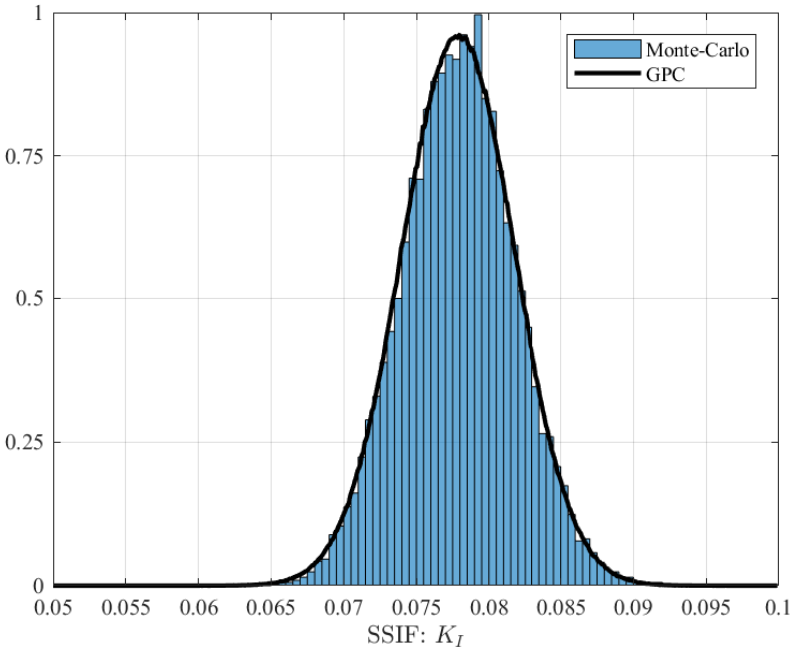

Figure 8: Normalized histogram displaying the Monte-Carlo results for the SSIF K_I and the probability density function of K_I computed using the GPC.

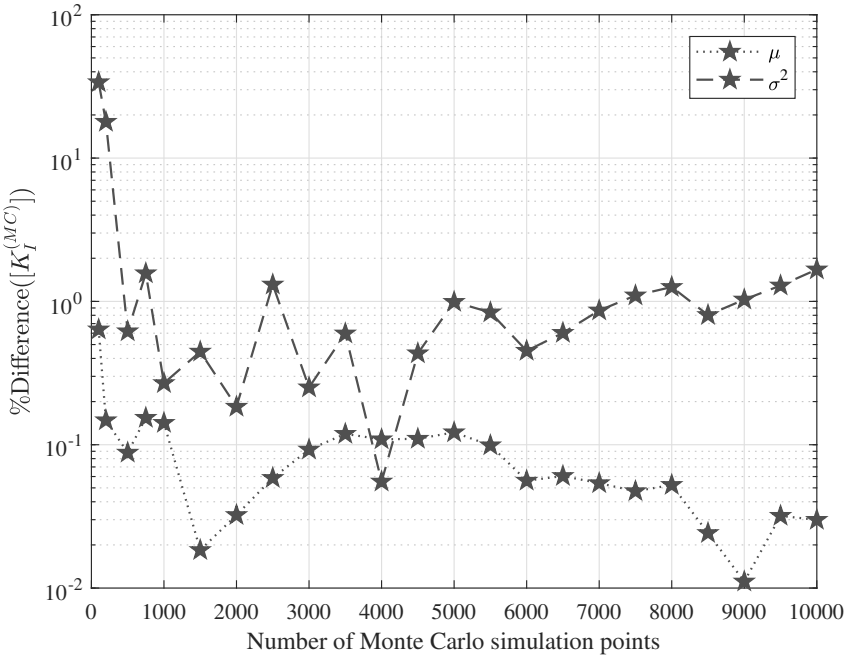

Figure 9: Relative difference of the mean value & the variance of the SSIF computed using increasing number of Monte-Carlo points vs. the SSIF computed using the GPC method, (33).

4.3. A cracked domain with a stochastic Poisson ratio & displacements boundary conditions

Same circular cracked domain as in Section 4.1 with traction free boundary conditions on crack faces is considered, having a deterministic Young modulus and a stochastic Poisson ratio:

$$E = 1, \quad \nu = 0.3 + 0.03\xi$$
$$\xi \sim \mathcal{N}(0,1), \quad f_\xi(t) = \frac{1}{\sqrt{2\pi}} e^{-\frac{t^2}{2}} \tag{38}$$

Essential boundary conditions are prescribed on the circular boundary $u_\theta(r=1) = \cos(\frac{\theta}{2})$, such that only Mode I is excited.

We follow again the steps detailed in Section 4.1 so to compute the SSIF by using the GPC representation of the the eigenfunctions. We then compute $A_1(\xi)$ and the SSIF $K_I(\xi)$ at several arbitrary selected points in the domain that all provide same stochastic SSIF:

$$K_I = 0.07434621 + 0.02506838\xi \tag{39}$$

The third moment obtained is $-1.65270616 \cdot 10^{-5}$ (skewness: -1.04909968) and the fourth moment obtained is $2.11034864 \cdot 10^{-7}$ (kurtosis: 5.34378552). Using the J-integral (at $R = 0.1$), the finite element method and the Monte-Carlo method, we extract the SSIF $K_I(\xi)$ for 10000 different choices of Poisson ratios, according to the stochastic behavior of $\nu(\xi)$, (38). The results of $K_I(\xi)$ obtained at the 10000 samples are converged in both the mean value (less then 0.04%) and the variance (less then 0.06%). The PDF of the obtained SIF using both the GPC method and the Monte-Carlo method is presented in Figure 10.

The relative difference of the mean value of the SSIF computed using Monte-Carlo method compared with the GPC method (equation (33)) is presented in Figure 11. Results show that the relative difference obtained is less then 0.5%.

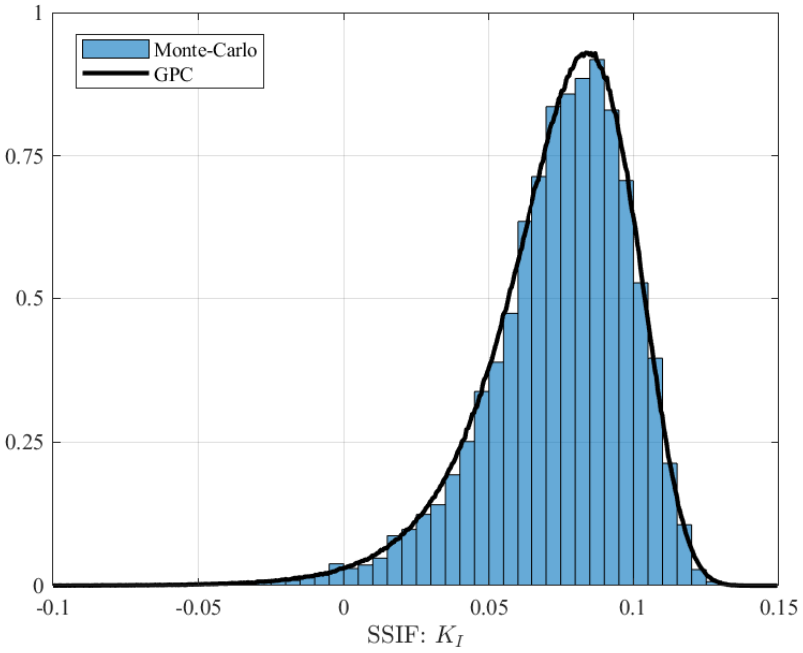

Figure 10: Normalized histogram displaying the Monte-Carlo results for the SSIF K_I and the probability density function of K_I computed using the GPC.

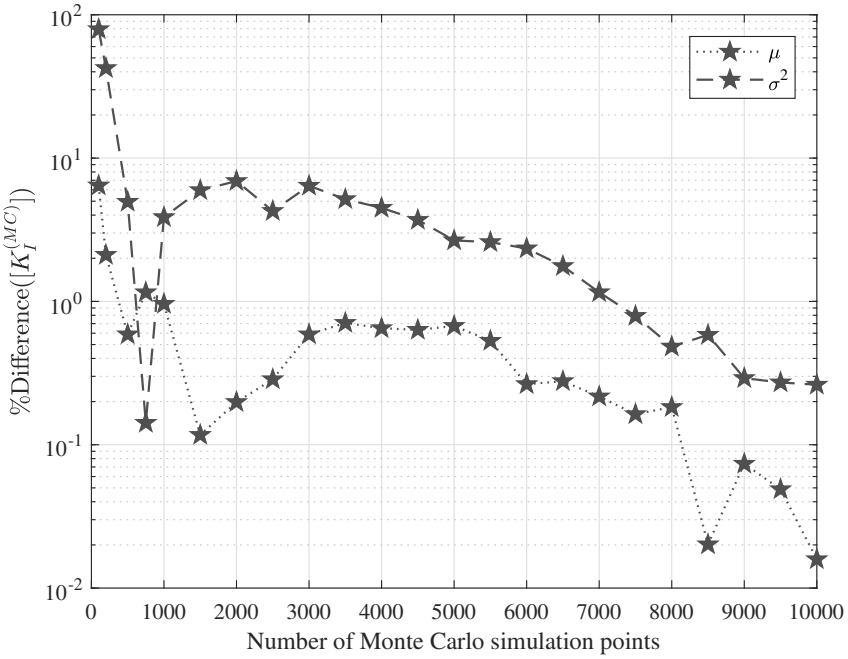

Figure 11: Relative difference of the mean value & the variance of the SSIF computed using increasing number of Monte-Carlo points vs. the SSIF computed using the GPC method, (33).

4.4. A cracked CTS domain with a stochastic Poisson ratio & traction boundary conditions

Consider the classical CTS as shown in Figure 12 (all dimensions in cm). The CTS is subject to bearing loads at the tearing holes having an equivalent force in the X_2 direction as presented in Figure 13. All other faces are traction free. The specimen is subjected to a tension load of 100 N/cm distributed over hole's upper surface such that only Mode I is excited in the vicinity of the crack tip. The domain is discretized using a p-FEM mesh, with geometrical progression towards the singular point with a factor of 0.15 where the smallest layer in the vicinity of the tip is at $r = 0.15^3$.

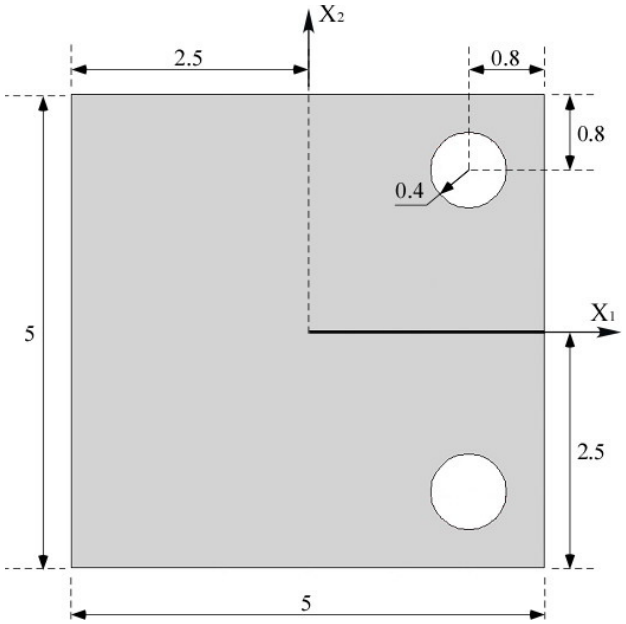

Figure 12: The Compact Tension Specimen (CTS). Dimensions in cm.

Material properties considered herein are deterministic Young modulus and stochastic poisson ratio given by equation (38). We follow the steps detailed in Section 4.1 so to compute the eigenfunctions and the displacements by using the GPC representation. We extract $A_1(\xi)$ and then compute the SSIF $K_I(\xi)$ at several arbitrary selected points. All computations provide the same SSIF, having the mean & variance:

$$\begin{aligned} \mu[K_I(\xi)] &= 361.23970637 \\ \sigma^2[K_I(\xi)] &= 7.11650081 \cdot 10^{-6} \end{aligned} \tag{40}$$

The third moment obtained is $-6.69843175 \times 10^{-9}$ (skewness -0.35283651) and the fourth moment is $1.43276236 \times 10^{-10}$ (kurtosis 2.82905460). The results indicate a deterministic

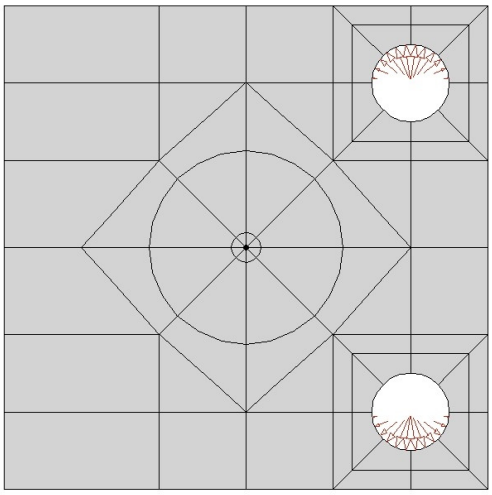

Figure 13: p-FEM model of the CTS with a bearing load at the two holes.

SSIF due to the small value of the variance compared to the large value of the mean value, as expected according to Theorem 2a.

Using the J-integral, the finite element method and Monte-Carlo method, we extract the SIF $K_I(\xi)$ for 10000 different choices of Poisson ratio, according to the stochastic behavior of $\nu(\xi)$, (38). All choices of Poisson ratio provide the exact same SSIF.

The relative difference of the mean value of the SSIF computed using Monte-Carlo method compared with the GPC method (equation (33)) is presented in Figure 14. Results show a relative difference of less than 0.05%.

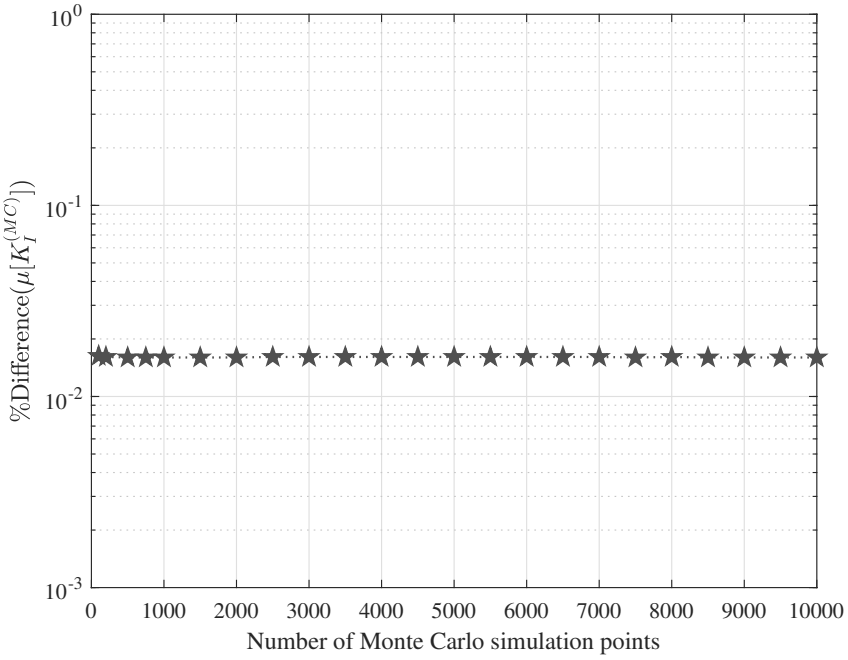

Figure 14: Relative difference of the mean value of the SSIF computed using increasing number of Monte-Carlo simulations vs. the SSIF computed using the GPC method, (33).

5. Summary and Conclusions

The elastic asymptotic solution in the vicinity of a traction free crack tip, in a 2D domain having stochastic isotropic material properties, was investigated. In case of stochastic $E(\xi)$ or $\nu(\xi)$, where ξ is a random variable, the eigenvalues remain deterministic however the eigenfunctions, A_i coefficients, displacements, stresses and stress intensity factors K_i may be stochastic. The explicit stochastic representation of each depends on the stochastic material property as well as on the boundary conditions on the far away boundary. Four explicit asymptotic series representations were presented that were classified by the material property stochasticity and type of far boundary conditions.

The generalized polynomial chaos (GPC) method was thereafter used to approximate the stochastic behavior of the eigenfunctions, which in addition to the computed $A_i(\xi_k)$ (using deterministic FEAs for a given finite number of material properties), allowed the determination of $A_i(\xi)$ and SSIFs. The method uses standard deterministic FEA, and converges extremely fast in the stochastic space as the number of Hermite polynomials increased and number of Hermie-Gauss integration points increased.

Four different example problems were presented for which SSIFs were computed by the GPC and compared to these obtained using the classical Monte-Carlo method. The relative difference between the methods indicate that the proposed method is accurate and efficient (almost two orders of magnitude more efficient compared to the classical MC method).

The presented methods may be extended to address two open questions in a future investigation:

- The explicit stochastic approximation of the SSIFs $K_I(\xi_1, \xi_2)$ & $K_{II}(\xi_1, \xi_2)$ when both of material properties are stochastic and may be described by two iid random variables having different PDFs.

- Possible stochastic representation of the eigenvalues for V-notch singularities and the associated generalized SSIFs.

Acknowledgements

ZY gratefully acknowledges the support of this research by the Israel Science Foundation (grant No. 593/14).

[1] R. Ghanem and P. Spanos. *Stochastic finite elements: A spectral approach*. Springer-Verlag Publishers, 1991.

[2] D. Xiu. *Numerical methods for stochastic computations: A spectral method approach*. Princeton University Press, 2010.

[3] S. Rahman. Probabilistic fracture mechanics: j-estimation and finite element methods. *Engrg. Frac. Mech.*, 68:107–125, 2001.

[4] B.N. Rao and S. Rahman. Probabilistic fracture mechanics by galerkin meshless methods part i: rates of stress intensity factors. *Comput. Mech.*, 28:351–364, 2002.

[5] M.S. Chowdhury, C. Song, and Gao W. Probabilistic fracture mechanics by using monte carlo simulation and the scaled boundary finite element method. *Engrg. Frac. Mech.*, 78:2369–2389, 2011.

[6] R.M. Reddy and B.N. Rao. Stochastic fracture mechanics by fractal finite element method. *Computer Meth. Appl. Mech. Engrg.*, 198:459–474, 2008.

[7] C. Su and C. Zheng. Probabilistic fracture mechanics analysis of linear-elastic cracked structures by spline fictitious boundary element method. *Engineering Analysis with Boundary Elements*, 36:1828–1837, 2012.

[8] Andre Teofilo Beck and Wellison Jose de Santana Gomes. Stochastic fracture mechanics using polynomial chaos. *Probabilistic Engineering Mechanics*, 34:26 – 39, 2013.

[9] V.V. Silberschmidt. Effect of material's randomness on scaling of crack propagation in ceramics. *Int. Jour. Fracture*, 140:73–85, 2006.

[10] Ö. Keleş, García R.E., and K.J. Bowman. Stochastic failure of isotropic, brittle materials with uniform porosity. *Acta Materialia*, 61:2853–2862, 2013.

[11] M. Costabel, M. Dauge, and Z. Yosibash. A quasidual function method for extracting edge stress intensity functions. *SIAM Jour. Math. Anal.*, 35(5):1177–1202, 2004.

[12] Z. Yosibash, N. Omer, M. Costabel, and M. Dauge. Edge stress intensity functions in polyhedral domains and their extraction by a quasidual function method. *Int. Jour. Fracture*, 136:37 – 73, 2005.

[13] N. Omer and Z. Yosibash. Edge singularities in 3-D elastic anisotropic and multi-material domains. *Computer Meth. Appl. Mech. Engrg.*, 197:959–978, 2008.

[14] M. L. Williams. Stress singularities resulting from various boundary conditions in angular corners of plates in extension. *Trans. ASME, Jour. Appl. Mech.*, 19:526–528, 1952.

[15] Z. Yosibash. *Singularities in Elliptic Boundary Value Problems and Elasticity and their Connection with Failure Initiation*. Springer, 2012.

[16] J.R. Rice. A path independent integral and the approximate analysis of strain concentration by notches and cracks. *Journal of Applied Mechanics*, 35(2):379–386, June 1968.